TECHNISCHE MECHANIK, Band 28, Heft 1, (2008), 32– 42
Manuskripteingang: 31. August 2007

Towards Multiscale Computation of Confined Granular Media - Contact Forces, Stresses and Tangent Operators -

H. A. Meier, P. Steinmann, E. Kuhl

The present work is focused on the computational simulation of granular media on different scales. On the mircoscopic level, we suggest a discrete element method to evaluate inter-particle contact forces. On the macroscopic level, we utilize the finite element method to determine stress distributions in a continuum sense. To bridge the gap between both scales, we apply the concept of a representative volume element, essentially linking both scales through the Taylor assumption and Hills' theorem. The governing equations on both scales will be presented with a particular focus on the consistent linearization of the nonlinear response on the material point level. The latter essentially allows for the use of the highly efficient Newton Raphson scheme which ensures quadratic convergence of the iterative solution process. We first elaborate the influence of the size of the representative volume element in terms of a contact normal density function and statistical error bar analyzes. Then we demonstrate the features of our multiscale algorithm in terms of the classical slope stability benchmark problem.

1 Introduction

Multiscale modeling of confined granular media opens a novel way of simulating and understanding the complicated behavior of granular structures. Standard continuum methods are not capable of reproducing distinguishing manners of granular media, i.e., the breaking and forming of particle contacts. Instead, a two scale homogenization procedure, containing the discrete element method (dem) and the finite element method (fem), allows the capture of such distinguishing manners, see Dettmar (2006). Thereby, a representative volume element (rve), containing the discrete granular structure, is introduced on the microscale level. The macroscale is discretized by finite elements. The dem as well as the fem form a perfect alliance in the context of computational confined granular media. The dem, introduced by Cundall and Strack (1978, 1979), is suitable to capture the behavior of granular aggregates. Its drawback is its high computational cost, which limits the number of grains in the calculation. The fem, having low up to moderate computational cost, resembles the perfect base to include the dem on the gauss point level. In such a multiscale combination, the number of grains is limited inside the rve and the drawback of the dem disappears naturally. Up to this point, the homogenization cycle was limited to the application of a macroscopic deformation gradient on the rve on the micro level and returning the related stress measure, see, e.g., Kaneko et al. (2003); Dettmar (2006). Studies pertaining the macroscopic stress and strain formulation are found in the publication of Kruyt and Rothenburg (1996); Kuhl et al. (2000); D'Addetta et al. (2001); Ehlers et al. (2001, 2003). However, the macroscopic finite element calculation typically relies on the calculation of two quantities on the material point level: the stress tensor and the tangent operator. Thus, due to the missing tangent operator, a rather cumbersome macroscale computation was applied. Typically, an explicit dynamic relaxation scheme was used on the macroscale level, bringing along high computational costs.
In this manuscript we point out a way to circumvent high computational costs by introducing a consistent tangent operator. Thus, we are capable of applying a Newton type iteration scheme on the macroscale level. This contribution solely focuses on the assumption of Taylor and Voigt (1889). Hence, we do not consider any kind of fluctuations on the microscale level. All particles are mapped by the macroscopic deformation gradient tensor, leading to a homogeneous microscale deformation. Clearly, no relaxation procedure is used on the microscale level. Although this assumption includes the drawback of disregarding any effects of the morphology of the granular assembly, as noted in Larsson and Runesson (2007), the low computational costs and with this the possibility of performing large scale computations are considered to be attractive. The Piola stress as well as the consistent tangent operator are derived from the overall macroscopic energy, ab initio guaranteeing a major symmetry of the tangent operator.
The publication is segmented as follows: The calculation of the inter particle contact forces is presented in Section 2. Therefore, a force potential function is introduced which depends on the particle overlap. Section 3 concerns

the homogenization process, based on the averaged macroscopic energy, resulting in the definition of the averaged macroscopic stress and tangent operator. To ensure the representativeness of the used volume element, a basic deformation rve study is outlined in Section 4. Uniformity of the initial contact network is compared by a contact normal density function and by characteristic error bar analyzes. A final example based on the well-known slope stability benchmark problem is illustrated in Section 5. Lastly, section 6 closes with a final discussion.

2 Microscale - Contact Force

The map between the initial particle positions $\boldsymbol{X}_i$ and the current particle positions $\boldsymbol{x}_i$ is accomplished by the macroscopic deformation gradient tensor $\overline{\boldsymbol{F}}$.

$$\boldsymbol{x}_i = \overline{\boldsymbol{F}} \cdot \boldsymbol{X}_i \tag{1}$$

Quantities superimposed by an over bar are related to the macroscale level. The mapping procedure, as shown in (1), reflects the assumptions of Taylor and Voigt (1889), i.e., assuming a homogeneous deformation field over the entire granular assembly on the microscopic scale. Thus, the position of each granule is solely described by the macroscopic deformation gradient tensor $\overline{\boldsymbol{F}}$, while individual particle fluctuations are ignored. This assumption compares to the Cauchy-Born rule in continuum-atomistics, see, e.g., Cauchy (1828a,b); Born (1915). By sub-

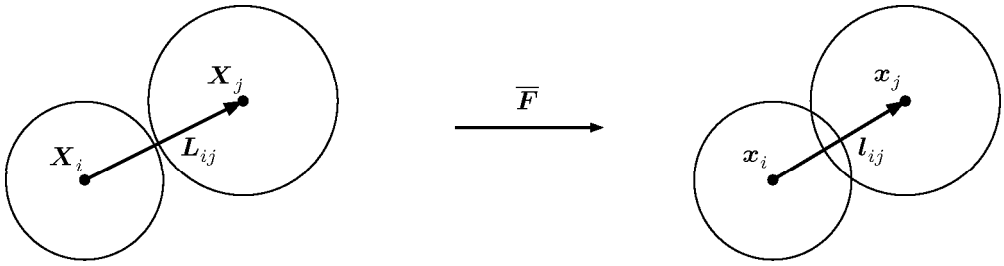

Figure 1: Initial and deformed configuration of the particles i and j. Left: Initial configuration with ε_{ij} less than zero. The branch vector $\boldsymbol{L}_{ij}$ connects the centers of the particles i and j. Right: Current configuration with an overlap ε_{ij} greater than zero. The particles i and j are in contact. The branch vector $\boldsymbol{l}_{ij}$ relates the two particle centers.

tracting the position vectors of two particles i and j we derive the branch vector $\boldsymbol{l}_{ij}$ which connects the particle centers in the current deformed configuration, see Fig. 1.

$$\boldsymbol{l}_{ij} = \boldsymbol{x}_j - \boldsymbol{x}_i = \overline{\boldsymbol{F}} \cdot \left[\boldsymbol{X}_j - \boldsymbol{X}_i \right] = \overline{\boldsymbol{F}} \cdot \boldsymbol{L}_{ij} \tag{2}$$

The length of the branch vector $\boldsymbol{l}_{ij}$ is employed to calculate the overlap ε_{ij} between the particles i and j.

$$\varepsilon_{ij} = r_i + r_j - \left|\left| \boldsymbol{l}_{ij} \right|\right| \tag{3}$$

Thereby, the radii of the particles i and j are denoted by r_i and r_j, respectively. For a zero or positive value of ε_{ij} particle i and j are considered to be in contact and are able to transmit forces. Accordingly, a negative value of ε_{ij} signals a gap of the size $|\varepsilon_{ij}|$. Equation (3) is thus considered as the contact condition between the particles i and j. Next, we introduce a force-potential function Φ_{ij} which depends on the overlap ε_{ij}, see, e.g., Miehe and Dettmar (2004); Zohdi (2005). We require the force-potential function to be convex and its derivative monotonously increasing. Additionally, we demand its derivative to be zero for ε_{ij} being zero itself. Thus, we implicitly enforce the constraint $\varepsilon_{ij} < 0$.

$$\Phi_{ij} = \frac{E_{\mathsf{n}ij}}{2} \left[\mathscr{H}(\varepsilon_{ij})\, \varepsilon_{ij} \right]^2 \tag{4}$$

Herein, $E_{\mathsf{n}ij}$ stands for the contact normal stiffness between the particle i and j, whereas $\mathscr{H}$ represents the Heaviside function. The Heaviside function of ε_{ij} enforces the previously introduced requirements of the force-potential function Φ_{ij}. By using the introduced force-potential function, we thus restrict our method to repulsive

forces, usually found in the context of dry granular media. Performing the derivative of (4) with respect to the position of particle i leads to the normal contact force $\boldsymbol{f}_{ij}$, acting on particle i.

$$\boldsymbol{f}_{ij} = -\frac{\mathrm{d}\,\Phi_{ij}}{\mathrm{d}\,\boldsymbol{x}_i} = -E_{\mathsf{n}ij}\;\mathscr{H}\big(\varepsilon_{ij}\big)\,\varepsilon_{ij}\,\boldsymbol{n}_{ij} \tag{5}$$

The magnitude of the normal contact force is defined by $-E_{\mathsf{n}ij}\;\mathscr{H}\big(\varepsilon_{ij}\big)\,\varepsilon_{ij}$, while its direction is given by the contact normal $\boldsymbol{n}_{ij} = \boldsymbol{l}_{ij} \,/\, \big|\big|\boldsymbol{l}_{ij}\big|\big|$. The complete particle assembly can be compared to a network of linear springs, see Hrennikoff (1941). In contrast to the work of Hrennikoff, however, the contact network between the particles is developed and altered continuously during the simulation.

3 Macroscale - Stress and Tangent Moduli

The starting point of the homogenization procedure is the well known energy averaging theorem by Hill (1972). This theorem, also known as Hill-Mandel condition, requires the macroscopic energy $\overline{\Phi}$ to be equivalent to the volume average of the energy in the rve on the microscale level $\langle\,\Phi\,\rangle$, see , i.e., Zohdi and Wriggers (2005). The averaging procedure itself is denoted by a pair of triangular parenthesis.

$$\overline{\Phi}\;\big(\overline{\boldsymbol{F}}\,\big) \;=\; \big\langle\,\Phi\;\big(\varepsilon_{ij}\;\big(\overline{\boldsymbol{F}}\,\big)\big)\big\rangle = \frac{1}{2\mathsf{V}_{\mathsf{rve}}}\sum_{i=1}^{\mathsf{nop}}\sum_{\substack{j=1\\ j\neq i}}^{\mathsf{nop}}\Phi_{ij}\;\big(\varepsilon_{ij}\,\big)\,, \tag{6}$$

where $\mathsf{V}_{\mathsf{rve}}$ denotes the volume of the rve in the undeformed reference configuration and

$$\begin{aligned}\big\langle\,\Phi\;\big(\overline{\boldsymbol{F}}\,\big)\big\rangle \;&=\; \frac{1}{4\mathsf{V}_{\mathsf{rve}}}\sum_{i=1}^{\mathsf{nop}}\sum_{\substack{j=1\\ j\neq i}}^{\mathsf{nop}}E_{\mathsf{n}ij}\;\big[\,\mathscr{H}\big(\varepsilon_{ij}\big)\,\varepsilon_{ij}\,\big]^2\\ &=\; \frac{1}{4\mathsf{V}_{\mathsf{rve}}}\sum_{i=1}^{\mathsf{nop}}\sum_{\substack{j=1\\ j\neq i}}^{\mathsf{nop}}E_{\mathsf{n}ij}\;\mathscr{H}\big(\varepsilon_{ij}\big)\,\big[r_i + r_j - \big|\big|\overline{\boldsymbol{F}}\;\boldsymbol{\cdot}\;\boldsymbol{L}_{ij}\,\big|\big|\big]^2\,.\end{aligned} \tag{7}$$

Since the indices i as well as j take values from 1 to the number of particles (nop), each particle contact is considered twice, i.e., we obtain twice the energy. Remedy is found by dividing the volume average of the energy by two. Insertion of (3) and (4) into (6) leads to the result presented in (7). Again, we would like to recall that the volume averaged microscopic energy merely depends on the macroscopic deformation gradient tensor $\overline{\boldsymbol{F}}$, based on the Taylor assumption. To obtain the macroscopic Piola stress $\overline{\boldsymbol{P}}$, which forms a work conjugated set with the macroscopic deformation gradient tensor $\overline{\boldsymbol{F}}$, we follow the standard procedure of deriving the macroscopic energy $\overline{\Phi}$ with respect to the macroscopic deformation gradient tensor.

$$\overline{\boldsymbol{P}}\;\big(\overline{\boldsymbol{F}}\,\big) \;=\; \frac{\mathrm{d}\,\big\langle\,\Phi\;\big(\overline{\boldsymbol{F}}\,\big)\big\rangle}{\mathrm{d}\,\overline{\boldsymbol{F}}} \tag{8}$$

with

$$\begin{aligned}\overline{\boldsymbol{P}}\;\big(\overline{\boldsymbol{F}}\,\big) \;&=\; \frac{1}{4\mathsf{V}_{\mathsf{rve}}}\sum_{i=1}^{\mathsf{nop}}\sum_{\substack{j=1\\ j\neq i}}^{\mathsf{nop}}E_{\mathsf{n}ij}\;\frac{d\;\mathscr{H}\big(\varepsilon_{ij}\big)\,\big[r_i + r_j - \big|\big|\overline{\boldsymbol{F}}\;\boldsymbol{\cdot}\;\boldsymbol{L}_{ij}\,\big|\big|\big]^2}{d\;\overline{\boldsymbol{F}}}\\ &=\; -\frac{1}{2\mathsf{V}_{\mathsf{rve}}}\sum_{i=1}^{\mathsf{nop}}\sum_{\substack{j=1\\ j\neq i}}^{\mathsf{nop}}E_{\mathsf{n}ij}\;\mathscr{H}\big(\varepsilon_{ij}\big)\,\varepsilon_{ij}\,\boldsymbol{n}_{ij}\otimes\boldsymbol{L}_{ij}\,.\end{aligned} \tag{9}$$

Using (5) we can rewrite (9) in a compact form,

$$\overline{\boldsymbol{P}}\;\big(\overline{\boldsymbol{F}}\,\big) \;=\; \frac{1}{2\mathsf{V}_{\mathsf{rve}}}\sum_{i=1}^{\mathsf{nop}}\sum_{\substack{j=1\\ j\neq i}}^{\mathsf{nop}}\boldsymbol{f}_{ij}\otimes\boldsymbol{L}_{ij}\,, \tag{10}$$

solely consisting of the normal contact forces $\boldsymbol{f}_{ij} = -E_{\mathrm{n}ij}\, \mathscr{H}(\varepsilon_{ij})\, \varepsilon_{ij}\, \boldsymbol{n}_{ij}$ of the current configuration as well as the branch vector $\boldsymbol{L}_{ij}$ of the initial configuration. A standard push-forward operation of the Piola stress results into the macroscopic Cauchy stress $\overline{\boldsymbol{\sigma}} = \left[1/\overline{J}\right] \overline{\boldsymbol{P}} \bullet \overline{\boldsymbol{F}}^{\,t}$ as

$$\begin{aligned} \overline{\boldsymbol{\sigma}}\,(\overline{\boldsymbol{F}}) &= \frac{1}{2\mathsf{V}_{\mathsf{rve}}} \sum_{i=1}^{\mathsf{nop}} \sum_{\substack{j=1 \\ j\neq i}}^{\mathsf{nop}} \boldsymbol{f}_{ij} \otimes \boldsymbol{l}_{ij} \\ &= -\frac{1}{2\mathsf{V}_{\mathsf{rve}}} \sum_{i=1}^{\mathsf{nop}} \sum_{\substack{j=1 \\ j\neq i}}^{\mathsf{nop}} E_{\mathrm{n}ij}\, \mathscr{H}(\varepsilon_{ij})\, \varepsilon_{ij}\, ||\boldsymbol{l}_{ij}||\, \boldsymbol{n}_{ij} \otimes \boldsymbol{n}_{ij}\,, \end{aligned} \tag{11}$$

whereby $\mathsf{v}_{\mathsf{rve}} = \overline{J}\, \mathsf{V}_{\mathsf{rve}}$ denotes the volume of the rve in the deformed configuration, with $\overline{J}$ being the determinant of $\overline{\boldsymbol{F}}$, relating the undeformed and the deformed rve volume. The macroscopic Cauchy stress reveals its symmetry by the dyadic product of the unit contact normal vectors. The second derivative of the averaged microscopic energy, presented in (7), with respect to the macroscopic deformation gradient tensor $\overline{\boldsymbol{F}}$ leads to the formulation of the two-field fourth order macroscopic algorithmic tangent operator $\overline{\boldsymbol{-}}$. In the structural mechanics literature, see for example Wriggers (2001), the first part of (12) would be denoted as the geometric part, $\overline{\boldsymbol{-}}^{\mathsf{geo}}$, resulting from the linearization of the non-linear finite kinematics, while the second part is typically denoted as the material part, $\overline{\boldsymbol{-}}^{\mathsf{mat}}$, obtained from the linearization of the non-linear constitutive equation. The explicit expressions of the geometric and material part of the macroscopic tangent operator are shown in (13). Nonlinearity due to the change of the contact network of the granular assembly is related to the material part of the tangent.

$$\overline{\boldsymbol{-}}\,(\overline{\boldsymbol{F}}) = \frac{\mathrm{d}^2 \left\langle \Phi\,(\overline{\boldsymbol{F}}) \right\rangle}{\mathrm{d}\,\overline{\boldsymbol{F}} \otimes \mathrm{d}\,\overline{\boldsymbol{F}}} = \frac{\mathrm{d}\,\overline{\boldsymbol{P}}\,(\overline{\boldsymbol{F}})}{\mathrm{d}\,\overline{\boldsymbol{F}}} = \overline{\boldsymbol{-}}^{\mathsf{geo}}\,(\overline{\boldsymbol{F}}) + \overline{\boldsymbol{-}}^{\mathsf{mat}}\,(\overline{\boldsymbol{F}}) \tag{12}$$

with

$$\begin{aligned} \overline{\boldsymbol{-}}^{\mathsf{geo}}\,(\overline{\boldsymbol{F}}) &= -\frac{1}{2\mathsf{V}_{\mathsf{rve}}} \sum_{i=1}^{\mathsf{nop}} \sum_{\substack{j=1 \\ j\neq i}}^{\mathsf{nop}} \frac{\mathscr{H}(\varepsilon_{ij})\, E_{\mathrm{n}ij}}{||\boldsymbol{l}_{ij}||} \varepsilon_{ij}\, \mathbf{1} \overline{\otimes} \left[\boldsymbol{L}_{ij} \otimes \boldsymbol{L}_{ij}\right] \\ \overline{\boldsymbol{-}}^{\mathsf{mat}}\,(\overline{\boldsymbol{F}}) &= \frac{1}{2\mathsf{V}_{\mathsf{rve}}} \sum_{i=1}^{\mathsf{nop}} \sum_{\substack{j=1 \\ j\neq i}}^{\mathsf{nop}} \frac{\mathscr{H}(\varepsilon_{ij})\, E_{\mathrm{n}ij}}{||\boldsymbol{l}_{ij}||} \left[r_i + r_j\right] \left[\boldsymbol{n}_{ij} \otimes \boldsymbol{n}_{ij}\right] \overline{\otimes} \left[\boldsymbol{L}_{ij} \otimes \boldsymbol{L}_{ij}\right] \end{aligned} \tag{13}$$

Please note the special dyadic product, $\{\bullet \,\overline{\otimes}\, \circ\}_{abcd} = \{\bullet\}_{ac} \otimes \{\circ\}_{bd}$, enforcing the major symmetry of $\overline{\boldsymbol{-}}$. Equivalent to the formula describing the macroscopic first Piola stress, the definition of the macroscopic algorithmic tangent operator $\overline{\boldsymbol{-}}$ depends exclusively on the macroscopic deformation gradient tensor $\overline{\boldsymbol{F}}$. The major as well as minor symmetry of the tangent is shown by a push-forward into the spatial configuration,

$$\begin{aligned} \overline{\boldsymbol{-}}\,(\overline{\boldsymbol{F}}) &= \frac{1}{J} \left[\mathbf{1} \overline{\otimes} \overline{\boldsymbol{F}}\right] \boldsymbol{:} \overline{\boldsymbol{-}} \boldsymbol{:} \left[\mathbf{1} \overline{\otimes} \overline{\boldsymbol{F}}^{\,t}\right] \\ &= \frac{1}{2\,\mathsf{v}_{\mathsf{rve}}} \sum_{i=1}^{\mathsf{nop}} \sum_{\substack{j=1 \\ j\neq i}}^{\mathsf{nop}} ||\boldsymbol{l}_{ij}||\, \mathscr{H}(\varepsilon_{ij})\, E_{\mathrm{n}ij} \left[\left[\left[r_i + r_j\right] \left[\boldsymbol{n}_{ij} \otimes \boldsymbol{n}_{ij}\right] - \varepsilon_{ij}\, \mathbf{1}\right] \overline{\otimes} \left[\boldsymbol{n}_{ij} \otimes \boldsymbol{n}_{ij}\right]\right]. \end{aligned} \tag{14}$$

The resulting expressions concerning the stresses as well as the tangent operators are related to the non-linear theory. Assuming small deformations on the microscale, as done in Luding (2004), quantities in the undeformed and deformed configuration are assumed to be equal. Including the presumption of the initial overlaps being equal

to zero, one can reproduce the results presented in Luding (2004, 2005),

$$\begin{aligned} \overline{\boldsymbol{\sigma}} &= \frac{1}{2\mathsf{V}_{\mathsf{rve}}} \sum_{i=1}^{\mathsf{nop}} \sum_{\substack{j=1 \\ j \neq i}}^{\mathsf{nop}} \boldsymbol{f}_{ij} \otimes \boldsymbol{l}_{ij} \\ \overline{} &= \frac{1}{2\mathsf{V}_{\mathsf{rve}}} \sum_{i=1}^{\mathsf{nop}} \sum_{\substack{j=1 \\ j \neq i}}^{\mathsf{nop}} ||\boldsymbol{l}_{ij}||^2 \, \mathscr{H}(\varepsilon_{ij}) \, E_{\mathsf{n}ij} \, \boldsymbol{n}_{ij} \otimes \boldsymbol{n}_{ij} \otimes \boldsymbol{n}_{ij} \otimes \boldsymbol{n}_{ij} \end{aligned} \quad , \tag{15}$$

where $\overline{}$ represents the linear elastic modulus and $\overline{\boldsymbol{\sigma}}$ is understood as the linear stress.

4 Microscale - Discrete Element Method

Let us first illustrate the discrete element solution on the integration point level. Although the focal point of this paper is the derivation of the macroscopic stress as well as the macroscopic tangent from the overall macroscopic energy, the need to select an appropriate rve is vital for any numerical example. A contact normal density function is used as a uniformity measure. This density function is closely related to the well-known rose diagram, introduced by Nightingale (1858), of the particle contact network. However, the contact normal density function offers a deeper insight and is not dependent on a fixed angle binning. Thus, we favor the approach of constructing a contact normal density function which is used to evaluate the generated rves in an efficient way. The rves under consideration are generated by the algorithm described in Meier et al. (2007). The generated rves incorporate

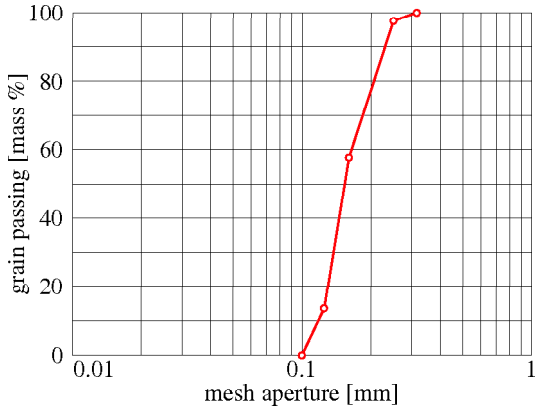

Figure 2: Typical grain size distribution for quartz sand used for rve generation. The grain passing in mass percent over mesh aperture is depicted. The abscissa shows the mesh aperture in [mm], whereas the ordinate reads the grain passing in volume percent.

the desired properties, including a geometric periodic boundary, a scaled prescribed grain size distribution, an unstructured particle setting and a high volume fraction. We select a grain size distribution for quartz sand as shown in Fig. 2 and generate five rves for a number of 70, 350 and 700 primary particles, depicted in Fig. 3. The corresponding contact normal density functions are shown in Fig. 3 as well. They are generated for an angle of influence equal to 10°, 20° as well as 30°. The influence of the different angles is clearly visible, e.g., a larger angle incorporates more contact normal vectors and thus results in a more uniform function. Naturally, in the case of a random distribution in space, a larger nop leads to a more uniform contact normal density function. While differences between the contact normal density functions for one rve alter strongly in the first two sets, the third set shows a good uniformity in most cases. A good agreement of the different contact normal density functions is found in the third image of set three. Thus, this rve is considered to behave in an isotropic manner for small deformations. In contrast, the third rve of set one will show an anisotropic behavior. Additional to the generation of the contact normal density function, which favors the third rve in set three, all rves are subjected to uniaxial compression as well as simple shear.
Error bar plots which show the volume average of the Cauchy stress versus the corresponding components of the deformation gradient are given in Fig. 4 and 5. While the compression test shows a good overall agreement for all rves, the results of the simple shear test differ significantly. In case of the compression test, a linear stress

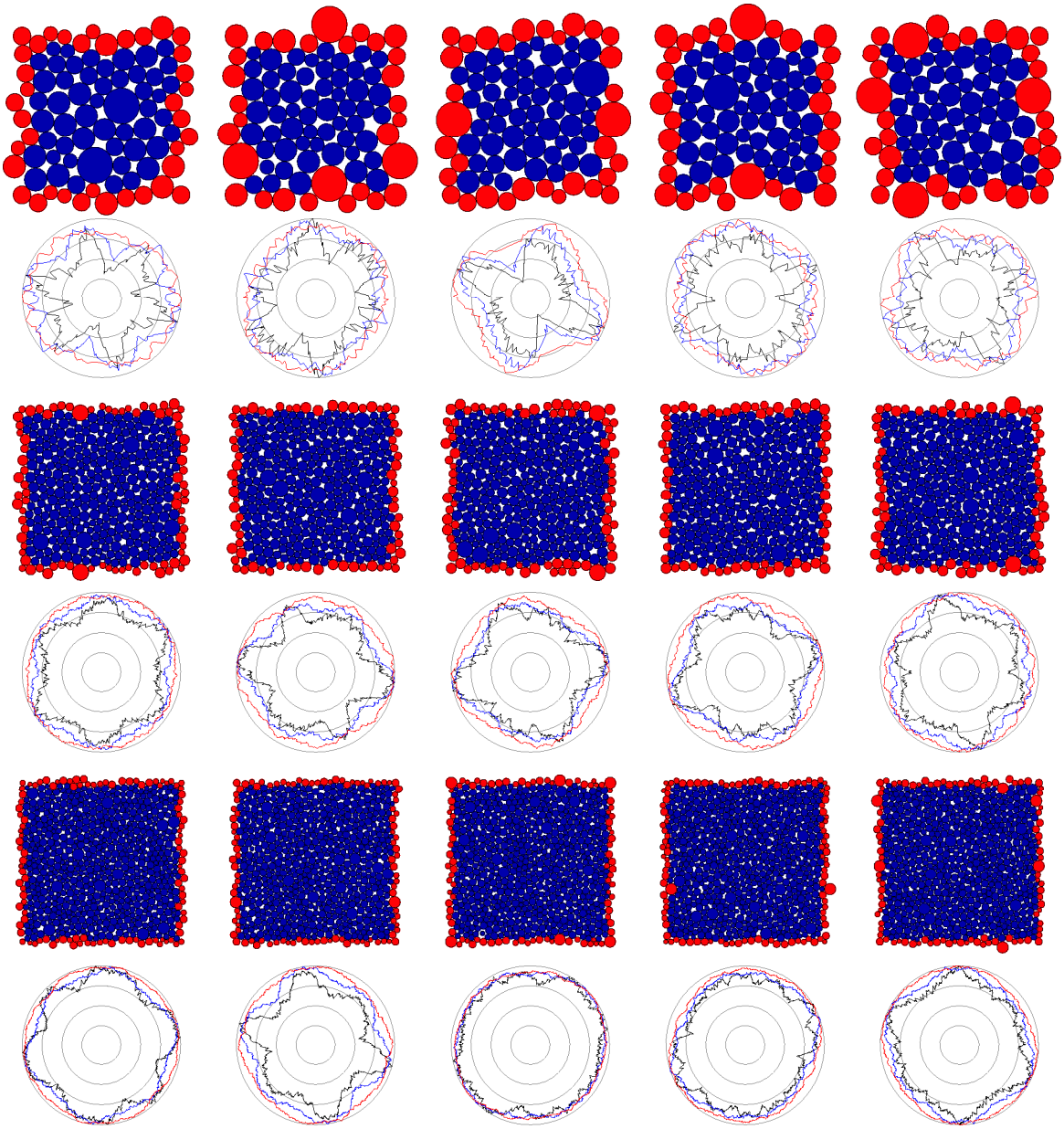

Figure 3: rves and their corresponding contact normal density functions. Black colored functions relate to an angle of influence equal to 10°, while blue and red colored functions correspond to an angle of influence equal to 20° and 30°, respectively. First set: Five rves, containing each 70 primary particles. Second set: Five rves, containing 350 primary particles. Third set: Five rves containing 700 primary particles.

behavior in the loading direction is observed, while in the orthogonal direction a nonlinear behavior is noticed. It is remarkable that for different nop the stress in the direction orthogonal to the direction of compression seems to converge towards to a meaningful overall function σ . Similar convergence is seen in the plot depicted in Fig. 5. In the case of the simple shear deformation a size reduction of the error bars, correlating to the increase of nop, is noticed. Please note, the coarse scale smoothness of the depicted stress curves is strongly related to the Taylor assumption. Therefore, if fluctuations on the microscale are considered, a non-smooth coarse scale behavior of the stress is observed, see Miehe and Dettmar (2004); Dettmar (2006). Nevertheless, fine scale non-smoothness is observed in both approaches. This observation is linked to minor changes inside the contact network.

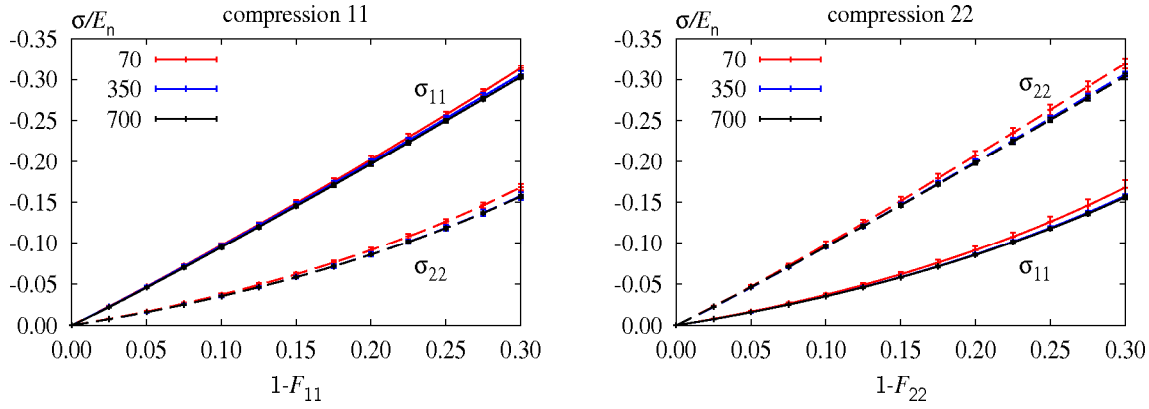

Figure 4: Averaged compression stress curves of the particle assemblies shown in Fig. 3. Error bars show the standard deviation. Left: Compression in 11 direction. Right: Compression in 22 direction. Solid lines relate to the Cauchy stress in 11 direction, while dashed lines are associated with the Cauchy stress in 22 direction.

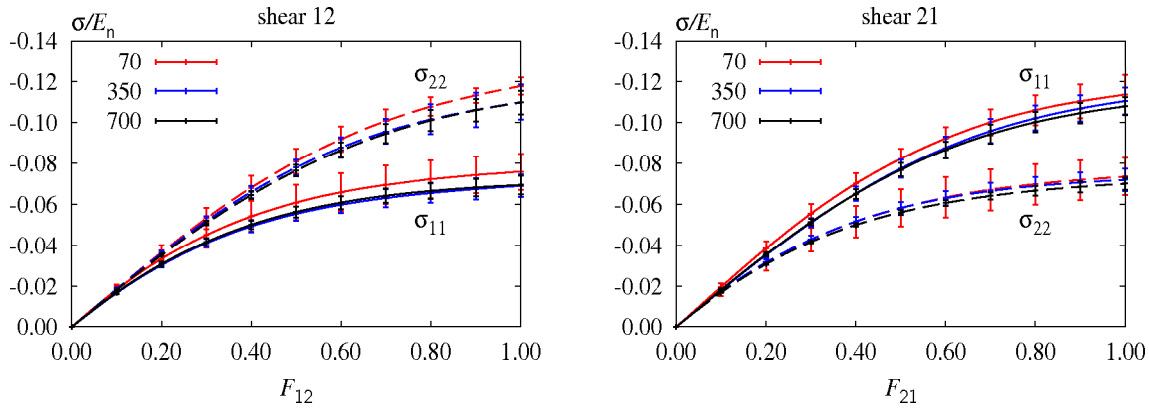

Figure 5: Averaged simple shear stress curves of the particle assemblies shown in Fig. 3. Error bars show the standard deviation. Left: Simple shear in 12 direction. Right: Simple shear in 21 direction. Solid lines relate to the Cauchy stress in 11 direction, while dashed lines are associated with the Cauchy stress in 22 direction.

5 Macroscale - Finite Element Method

The successful integration of the discrete element based rve simulation on the material point level implies the calculation of the macroscopic stress and tangent. It is illustrated by a representative finite element calculation. We analyze the slope stability problem, first discussed by Zienkiewicz and Pande (1977), subjected to dead load combined with a load originating from a massless strip footing subjected to an eccentric force. The dimensions of the problem as well as the applied boundary conditions are depicted in Fig. 6. Physical parameters are listed in Table 1. The footing has a width of 23.25 m. During the first load step, the structure is subjected to its dead load.

Table 1: Physical parameters for slope example

mass density	2.5E+03	$[kg/m^3]$
normal contact stiffness	2.8E+07	$[N/m^2]$
load	-4.0E+07	$[N]$

Twenty load steps, applying the load of the flexible footing, follow the initial load step. A related contour plot of the macroscopic von Mises stress as well as four deformed rves are shown in Fig 7. The von Mises stress computes by using the previous introduced Cauchy stress, $\overline{\boldsymbol{\sigma}}_{\text{mises}} = \sqrt{3/2\,\overline{\boldsymbol{\sigma}}^{\text{dev}} \bullet \overline{\boldsymbol{\sigma}}^{\text{dev}}}$, where $\overline{\boldsymbol{\sigma}}^{\text{dev}}$ denotes the deviatoric

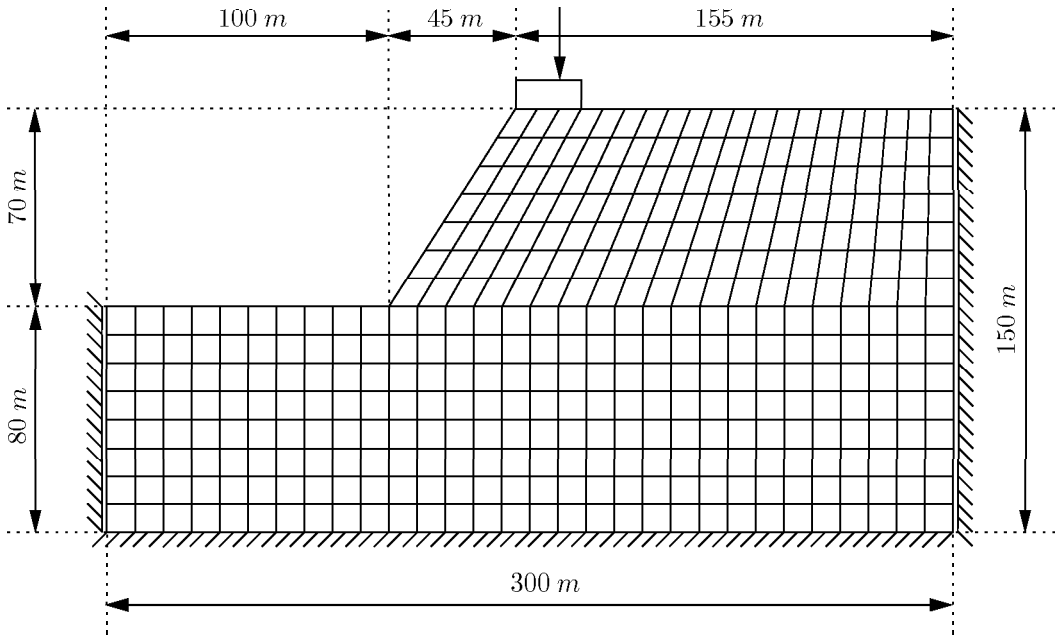

Figure 6: Undeformed mesh of the slope stability problem. Boundary conditions are depicted. 380 Q1 elements, containing each four Gauss points, are used. The massless footing is subjected to an eccentric force. The eccentricity is equal to 3.875 m.

part of the macroscopic Cauchy stress tensor. An initial localization, initiated at the maximum von Mises stress, is noted. The deformed rves incorporate their force networks. The line thickness of the branches corresponds to the magnitude of the contact normal force. Intuitively, one might think that the depicted microstructures are out of equilibrium and unstable. Nevertheless, based on the definition of the Taylor assumption, we do not demand the particles on the microscale to be in their equilibrium positions. However, this boundary condition guarantees the stability of the microscopic structure by definition. The convergence behavior of the relative energy norm for step two, six, eight, ten, fifteen and eighteen is listed in Table 2.

Table 2: Convergence behavior of the relative energy norm

iter	step 2	step 6	step 8	step 10	step 15	step 18
1	1.000E+00	1.000E+00	1.000E+00	1.000E+00	1.000E+00	1.000E+00
2	1.318E-02	3.341E-04	2.865E-04	3.940E-04	1.322E-03	4.817E-03
3	1.947E-04	2.308E-08	1.917E-08	1.503E-08	1.999E-07	3.816E-06
4	1.492E-07	7.110E-16	1.303E-16	7.415E-16	6.114E-14	7.276E-12
5	5.846E-13	3.441E-26	4.670E-26	5.014E-26	4.023E-26	5.932E-24
6	3.057E-26					

6 Summary and Discussion

The computational simulation of granular assemblies is a rather challenging and cumbersome task since granular materials are discrete in nature but yet consist of millions of particles which are expensive to trace individuallly. Following recent trends, we apply a multiscale simulation approach that captures individual contact forces on the microscopic scale and applies the concept of a representative volume element to characterize stresses on the macroscopic scale. Computationally speaking, we combine the discrete element method on the microscopic scale with the finite element method on the macroscopic scale.

To bridge the gap between the individual scales, we introduce a representative volume element and apply the classical Taylor assumption prescribing a homogeneous strain field to the discrete set of particles. We then solve the particle contact problem based on the discrete element method. The appropriate choice of the size of the underlying representative volume element has been discussed intensively in the recent literature. We thus decided to study

the rve size in terms of a contact normal density function and systematic errorbar analyses on the microscopic level before we move on to the multiscale approach. It turns out that the solution converges with increased particle numbers and that a few hundred particles seem a reasonable choice for the two dimensional simulations we have in mind.
Based on these preliminary studies, we then elaborated the overall finite element solution procedure. Existing multiscale models similar to the one we suggest have typically applied somewhat cumbersome solution techniques to solve the nonlinear finite element equations on the macroscopic scale. Instead of following the literature, we suggest to embed the overall solution in a classical Newton Raphson solution procedure. Accordingly, we illustrate the consistent linearization of the governing equations on the material point level lending itself to the algorithmic tangent operator which basically ensures quadratic convergence of the suggested solution scheme. Apart from the fact that each particle contact not only contributes to the overall stress but also to the overall tangent operator, the proposed algorithm is highly efficient and computationally cheap. It displays the characteristic properties of the classical Newton Raphson scheme and we were able to show its quadratic convergence for a typical finite element benchmark problem.
Nevertheless, we would like to point out that for a problem that is discrete in nature and essentially based on a continuous formation, removal and re-formation of inter-particle contacts, the overall solution is, of course, non-smooth. Technically speaking, although we have shown quadratic convergence of the Newton scheme in the present case, it might as well happen, that due to the transient re-structuring of the contact network, the global solution is in some sense too non-smooth for the overall solution technique to converge quadratically. These cases, however, are rather rare and can easily be avoided, e.g., by applying an adaptive time stepping scheme.
Finally, we would like to point out that although the presented algorithm has been proven highly effective and algorithmically efficient, it is far from being general enough to capture all characteristic effects in granular media. We are currently incorporating tangential contact forces that capture the effect of sliding on the microscopic level and naturally lend themselves to a plasticity model on the macroscopic scale. Moreover, we are analyzing different homogenization approaches that are more general than the classical Taylor assumption. In close collaboration with computer scientists, we are also trying to further improve efficiency to ultimately move to three dimensional simulations and develop powerful visualization techniques for the contact information on different scales.

References

Born, M.: *Dynamik der Kristallgitter*. Teubner (1915).

Cauchy, A. L.: De la pression ou tension dans un système de points matériels. *Exercises De Mathématiques*, pages 253–277.

Cauchy, A. L.: Sur l'équilibre et le mouvement d'un système de points matériels sollicités par des forces d'attraction ou de répulsion mutuelle. *Exercises De Mathématiques*, pages 227–252.

Cundall, P. A.; Strack, O. D. L.: The distinct element method as a tool for research in granular media. Tech. rep., Report to the National Science Foundation Concerning NSF Grant ENG76-20711, PART I (1978).

Cundall, P. A.; Strack, O. D. L.: The distinct element method as a tool for research in granular media. Tech. rep., Report to the National Science Foundation Concerning NSF Grant ENG76-20711, PART II (1979).

D'Addetta, G. A.; Kun, F.; Hermann, H. J.; Ramm, E.: *From solids to granulates - discrete element simulations of fracture and fragmentation processes in geomaterials*, pages 231–258. Continuous and Discontinuous Modelling of Cohesive Frictional Materials, Lecture Notes in Physics 586, Springer-Verlag, Berlin, Germany (2001).

Dettmar, J. P.: *Static and Dynamic Homogenization Analyses of Discrete Granular and Atomistic Systems on Different Time and Length Scales*. Ph.D. thesis, Institut für Mechanik (Bauswesen) , Universität Stuttgart (2006).

Ehlers, W.; Diebels, S.; Michelitsch, T.: *Microscopic modelling of granular materials taking into account particle rotations*, pages 259–274. Continuous and Discontinuous Modelling of Cohesive Frictional Materials, Lecture Notes in Physics 586, Springer-Verlag, Berlin, Germany (2001).

Ehlers, W.; Ramm, E.; Diebels, S.; D'Addetta, G. A.: From particle ensembles to cosserat continua: Homogenization of contact forces towards stresses and couple stresses. *Int. J. Solids and Structures*, 40, (2003), 6681–6702.

Hill, R.: On constitutive macro-variables for heterogeneous solids at finite strain. *Proc. R. Soc. Lond. A*, 326, (1972), 131–147.

Hrennikoff, A.: Solution of problems of elasticity by the framework method. *ASME J. Appl. Mech.*, 8, (1941), 169–175.

Kaneko, K.; Terada, K.; Kyoya, T.; Kishino, Y.: Global-local analysis of granular media in quasi-static equilibrium. *Int. J. Solids and Structures*, 40, (2003), 4043–4069.

Kruyt, N. P.; Rothenburg, L.: Micromechanical definition of the strain tensor for granular materials. *ASME Journal of Applied Mechanics*, 118, (1996), 706–711.

Kuhl, E.; D'Addetta, G. A.; Herrmann, H. J.; Ramm, E.: A comparison of discrete granular material models with continuous microplane formulations. *Granular Matter*, 2, (2000), 123–135.

Larsson, F.; Runesson, K.: RVE computations with error control and adaptivity: the power of duality. *Comput. Mech.*, 39, (2007), 647–661.

Luding, S.: Micro-macro transition for anisotropic, frictional granular packings. *Int. J. Sol. Struct.*, 41, (2004), 5821–5836.

Luding, S.: Anisotropy in cohesive, frictional granular media. *J. Phys.: Condens. Matter*, 17, (2005), 2623–2640.

Meier, H. A.; Kuhl, E.; Steinmann, P.: A note on the generation of periodic granular microstructures based on grain size distributions. *Int. J. Numer. Anal. Meth. Geomech.,(in press).*

Miehe, C.; Dettmar, J.: A framework for micro - macro transitions in periodic particle aggregates of granular materials. *Comput. Methods Appl. Mech. Engrg.*, 193, (2004), 225–256.

Nightingale, F.: *Notes on Matters Affecting the Health, Efficiency, and Hospital Administration of the British Army.* London: Harrison & Sons. (1858).

Voigt, W.: Über die Beziehungen zwischen den beiden Elastizitätskonstanten isotroper Körper. *Wied. Ann.*, 38, (1889), 573–587.

Wriggers, P.: *Nichtlineare Finite-Element-Methoden.* Springer-Verlag (2001).

Zienkiewicz, O. C.; Pande, G. N.: Time-dependent multilaminate model of rocks - a numerical study of deformation and failure rock masses. *Int. J. Anal. Meth. Geomech.*, 1, (1977), 219–247.

Zohdi, T. I.: Charge-induced clustering in multifield particulate flows. *Int. J. Numer. Meth. Engn.*, 62, (2005), 870–898.

Zohdi, T. I.; Wriggers, P.: *Introduction to computational micromechanics.* Springer-Verlag (2005).

Addresses: Holger A. Meier and Paul Steinmann, Department of Mechanical Engineering, University of Kaiserslautern, D-67653 Kaiserslautern, Germany. Ellen Kuhl, Department of Mechanical Engineering, Stanford University, Stanford, CA 95305-4040, USA.
email: homei@rhrk.uni-kl.de; ps@rhrk.uni-kl.de; ekuhl@stanford.edu.

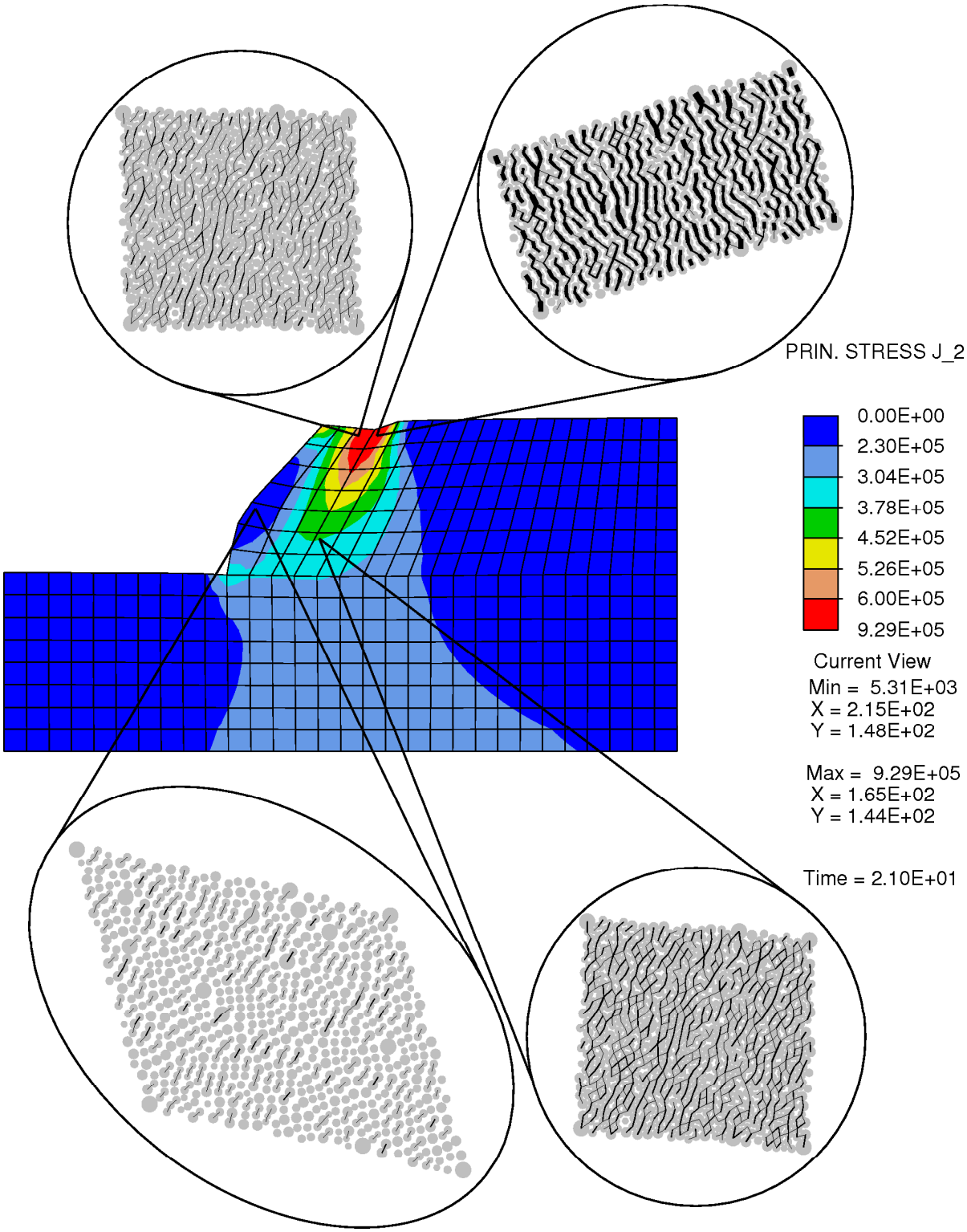

Figure 7: Final, deformed slope. The macroscopic von Mises stress is plotted, its minimum and maximum values as well as their locations are reported. Initial localization is visible. Four deformed rves containing their contact networks are depicted. The thickness of the branches corresponds to the magnitude of the contact forces. The scaling factors for the branch thickness as well as for the deformation are equal for all four particle plots.